J Neurophysiol 107: 1421–1430, 2012.
First published December 14, 2011; doi:10.1152/jn.00817.2011.

Fast reconfiguration of high-frequency brain networks in response to surprising changes in auditory input

Ruth M. Nicol,[1] Sandra C. Chapman,[1] Petra E. Vértes,[2] Pradeep J. Nathan,[2,3] Marie L. Smith,[4] Yury Shtyrov,[5] and Edward T. Bullmore[2,3]

[1]*Centre for Fusion, Space and Astrophysics, Department of Physics, University of Warwick, Coventry;* [2]*Behavioural and Clinical Neuroscience Institute, Department of Psychiatry, University of Cambridge, Cambridge Biomedical Campus, and* [3]*GlaxoSmithKline, Clinical Unit in Cambridge, Addenbrooke's Hospital, Cambridge;* [4]*Department of Psychological Sciences, Birkbeck, University of London; and* [5]*Medical Research Council Cognition and Brain Sciences Unit, Cambridge, United Kingdom*

Submitted 6 September 2011; accepted in final form 13 December 2011

Nicol RM, Chapman SC, Vértes PE, Nathan PJ, Smith ML, Shtyrov Y, Bullmore ET. Fast reconfiguration of high-frequency brain networks in response to surprising changes in auditory input. *J Neurophysiol* 107: 1421–1430, 2012. First published December 14, 2011; doi:10.1152/jn.00817.2011.—How do human brain networks react to dynamic changes in the sensory environment? We measured rapid changes in brain network organization in response to brief, discrete, salient auditory stimuli. We estimated network topology and distance parameters in the immediate central response period, <1 s following auditory presentation of standard tones interspersed with occasional deviant tones in a mismatch-negativity (MMN) paradigm, using magnetoencephalography (MEG) to measure synchronization of high-frequency (gamma band; 33–64 Hz) oscillations in healthy volunteers. We found that global small-world parameters of the networks were conserved between the standard and deviant stimuli. However, surprising or unexpected auditory changes were associated with local changes in clustering of connections between temporal and frontal cortical areas and with increased interlobar, long-distance synchronization during the 120- to 250-ms epoch (coinciding with the MMN-evoked response). Network analysis of human MEG data can resolve fast local topological reconfiguration and more long-range synchronization of high-frequency networks as a systems-level representation of the brain's immediate response to salient stimuli in the dynamically changing sensory environment.

graph theory; mismatch negativity (MMN), MEG; coherency; synchronization

NETWORK SCIENCE IS AN EMERGING mathematical field with applications across a wide range of physical systems. Since the early work by Erdös and Rényi (1959) to the pioneering papers of Watts and Strogatz (1998) and Barabási and Albert (1999), networks have emerged as a generally powerful way of quantifying complex systems as diverse as the nervous system of the nematode worm (*Caenorhabditis elegans*) (Bassett et al. 2010; Watts and Strogatz 1998) and the topology of the worldwide web (Barabási et al. 2000). In particular, graph theoretical analysis of network topology has grown rapidly in popularity as a way of modeling nervous systems. Graph analysis of brain networks is attractive, because the mathematical techniques are readily accessible and generalizable to many different scales and types and species of neuroscientific data—ranging from microelectrode recordings of local field potentials in animals to whole brain neuroimaging measurements of human brain structure or function (Bullmore and Sporns 2009). Moreover, many network properties quantified by graph analysis, such as efficiency of information transfer or topological modularity, are interpretable in the context of more general theories of information-processing networks (Bullmore and Bassett 2011).

Complex networks typically demonstrate a topological organization, which is neither completely random nor completely ordered (Newman 2003). Recently, it has been found that with the use of graph theoretical methods of analysis applied to neuroimaging data, such as structural and functional MRI (fMRI), EEG, and magnetoencephalography (MEG), structural and functional human brain networks share global topological properties in common with each other and with many other complex networks (Bassett and Bullmore 2006; Bullmore and Sporns 2009; Chialvo 2010; Eguíluz et al. 2005; Hagmann et al. 2008; Salvador et al. 2005). For example, human brain networks generally demonstrate the "small world" property of short path length (or high global efficiency) of connections between regional nodes anywhere in the brain, combined with high clustering (or high local efficiency) of connections between a clique of topologically neighboring nodes. Brain networks are also hierarchically modular with fat-tailed degree distributions, indicating the presence of high-degree network hubs (Achard et al. 2006; Meunier et al. 2010).

It is highly likely that the topological configuration of functional brain networks is dynamically reorganized in the context of changing environmental conditions or different experimental task demands (Bassett et al. 2006; Palva et al. 2010a, b). However, few studies have, so far, directly investigated the dynamics of human brain network topology. This has remained a methodologically challenging area. Spatially precise heomdynamic neuroimaging measurements, such as fMRI, do not measure neuronal dynamics directly and do not have subsecond time resolution: these technical limitations will clearly constrain what fMRI can reveal about network dynamics on the faster time scales, which are important for immediate perception, rapid action, and cognition. On the other hand, EEG and MEG measurements capture neuronal dynamics directly and can resolve high-frequency dynamics, but the anatomical sources of the surface-recorded signals are less well localized than fMRI time series. MEG offers some advantages over EEG in the precision of spatial localization, because the

Address for reprint requests and other correspondence: S. C. Chapman, Centre for Fusion, Space and Astrophysics, Dept. of Physics, Univ. of Warwick, Coventry, CV4 7AL, UK (e-mail: S.C.Chapman@warwick.ac.uk).

undistorted passage of magnetic field changes through brain tissue minimizes spatial blurring of sources recorded at neighboring sensors, whereas passage of electrical field changes is distorted by differential impedance of different tissue types, rendering surface EEG recordings more difficult to control for volume conduction effects (Hämäläinen et al. 1993).

MEG measurements of scalp magnetic-field potential can be used to construct binary or weighted graphs representing functional brain networks during performance of different tasks and at different points in time following presentation of experimental stimuli. Kitzbichler et al. (2011) recorded MEG during performance of working memory trials (each lasting 1.8 s), presented at various levels of difficulty, and demonstrated that more difficult versions of the task were associated with extensive reconfiguration of brain functional networks oscillating in the gamma (30–65 Hz) and beta (12–30 Hz) frequency intervals. Greater task difficulty was associated with greater global efficiency, reduced clustering, reduced modularity, and more long-distance synchronization between spatially remote MEG sensors, on average, over the course of a trial. Moreover, it was found that this pattern of network reconfiguration, considered compatible with the prior predictions of workspace theory (Baars 1988; Dehaene 2001), could be dynamically resolved on the order of 10 ms within the course of trials.

Here, we were interested in investigating changes in functional network organization, elicited not by sustained performance of an effortful task but by presentation of discrete, salient stimuli, which change somewhat unpredictably, as is usually the case in real life. Traditionally, neurocognitive mechanisms for processing of such transient, unexpected events have been investigated using the mismatch negativity (MMN) paradigm, a well-established experimental procedure in cognitive neuroscience and neurophysiology. In its simplest form, the participant listens passively as a predictable series of frequent—so-called standard—acoustic tones is presented, interspersed with occasional, unpredictable—so-called deviant—tones (Näätänen et al. 1978). The presentation of deviant tones, compared with standard tones, is associated with a time-locked, fronto-central negative peak in the EEG signal, occurring ~100–250 ms after stimulation, which also has a clear counterpart in MEG signals (Fig. 1). For acoustic changes, the main MMN generators are thought to be located in the lateral temporal auditory and frontal cortices (Alho 1995; Kujala and Näätänen 2010). This MMN-evoked response can be elicited without asking participants consciously to pay attention to auditory stimulation and is often regarded as a neurophysiological marker of automatic auditory discrimination or perceptual accuracy and short-term auditory memory or learning, reflecting the greater salience and depth of processing of the more surprising and infrequent stimuli. The MMN response has also been reported as abnormal in patients with cognitive impairment due to schizophrenia (Shelley et al. 1991, 1999) and Alzheimer's disease (Pekkonen et al. 1994).

There has been substantial prior work on the neurocognitive mechanisms of the MMN response (Garagnani et al. 2009; Garrido et al. 2009b). The model adjustment hypothesis is that the MMN response is a marker of changes in a distributed fronto-temporal network, whereas the adaptation hypothesis proposes that the signal is generated by more local processes of neuronal adaptation in the auditory cortex. Recent studies of experimental MEG data, using dynamic causal modeling (DCM) rigorously to compare candidate mechanistic models, have demonstrated that brain-connectivity changes underlying the MMN response include intra-areal adaptation in temporal cortex, as well as plasticity of interareal connections, e.g., between the frontal and temporal cortex (Garrido et al. 2008). This profile of both local and distributed systems reconfiguration was considered incompatible with either model adjustment or adaptation theories alone but could be accounted for by a more general theory based on prediction error coding (Baldeweg 2007; Garrido et al. 2009a).

We recorded neuromagnetic signals in response to variable tonal stimuli at 204 planar gradiometer MEG sensors in healthy volunteers and used the imaginary part of coherency, $Im(C_{ij})$,

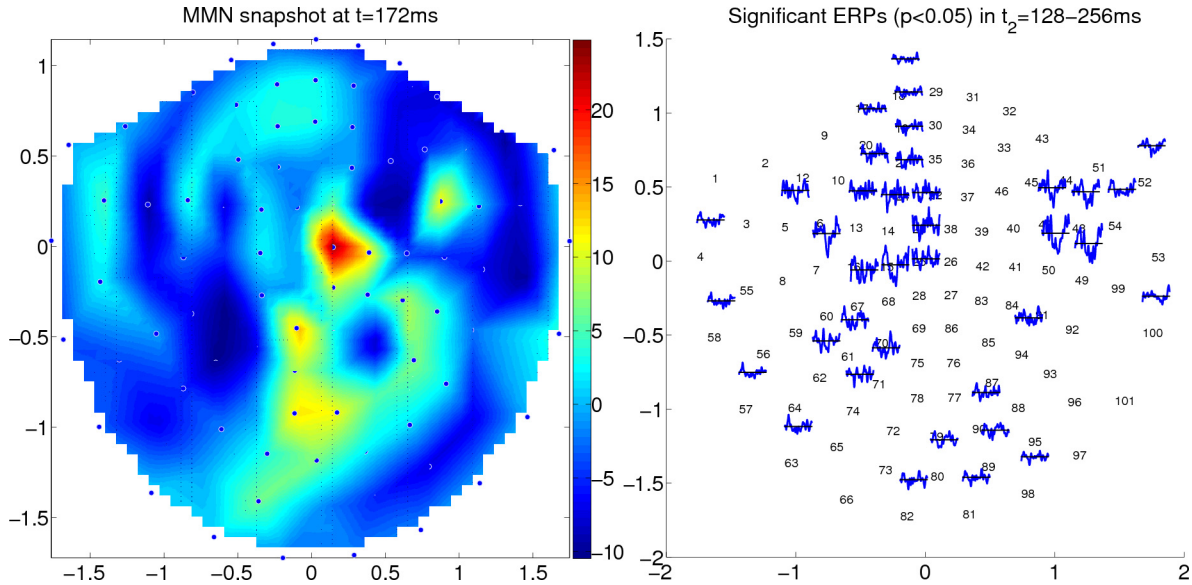

Fig. 1. The evoked response to deviant tones vs. standard frequency tones in the mismatch negativity (MMN) paradigm. *Left*: a snapshot of the difference in amplitude between tones (standard-deviant) averaged across all subjects at $t = 172$ ms. *Right*: significant ($P < 0.05$, false discovery rate corrected) evoked potentials [event-related potentials (ERPs)] are shown for the time interval $t_2 = 128$–256 ms. Note that a significant fronto-central deviation was observed in the expected time interval following presentation of tones.

to measure band-limited, functional connectivity between each pair of sensors, on average, over the course of <1 s, following presentation of each tone, and in contiguous, nonoverlapping time windows or epochs, each of 128 ms duration. We thresholded the functional connectivity matrices to generate binary or weighted graphs for topological analysis (Fig. 2). On the basis of prior theory and experimental results (Garrido et al. 2009a; Kitzbichler et al. 2011), we predicted that presentation of deviant acoustic tones would be associated with local and distributed changes in network organization compared with standard tones and that an analysis of network configuration over time would find that deviant-related network reconfiguration coincided with the time epoch of the MMN-evoked response.

METHODS

Sample. Sixteen healthy volunteers (mean age = 29 yr; range = 20–42 yr) were recruited from the healthy participant panel maintained by the GlaxoSmithKline Clinical Unit in Cambridge (UK). All participants were free of medication (including nicotine and drugs of abuse) and had no physical or psychiatric illness as assessed by a physician.

The study was approved by the Cambridgeshire Research Ethics Committee (07/H0306/120). All participants provided informed consent in writing and were reimbursed for their participation. The data reported here are part of a larger dataset collected as part of the same experimental protocol.

MMN paradigm. We used a multifeature version of the MMN paradigm (Kujala 2007; Näätänen et al. 2004), which presented a series of auditory stimuli, including 50% standard frequency tones of 330 ms duration (275 Hz and two harmonics), presented as every other trial in the sequence. These were interspersed randomly with deviant frequency trials, in which a tone was presented at 20% higher frequency than the standard tone. We focused here on the classical MMN response, which is defined by the experimental contrast between standard and deviant frequency simple tones. However, as part of this multifeature MMN paradigm, other deviant trial types were presented: a length deviant tone (20% longer than the standard frequency tone); two words: pipe and bite; and two pseudowords: pite and bipe. The experimental data recorded during presentation of nonstandard trials, other than the deviant frequency tone, are not reported here.

Each tonal stimulus was presented with an interstimulus interval of ~800 ms, measured from the onset of the simulus and jittered randomly in the range ±60 ms. All deviant stimuli were presented in a random order (although the same stimuli were never presented consecutively) and were always preceded and succeeded by a single standard tone. All deviant stimuli also had a similar occurrence rate of ~8%. Thus ~90 deviant frequency tones were presented in the course of each experiment. Participants heard these tones and words passively over a 20-min interval, while they watched a silent movie.

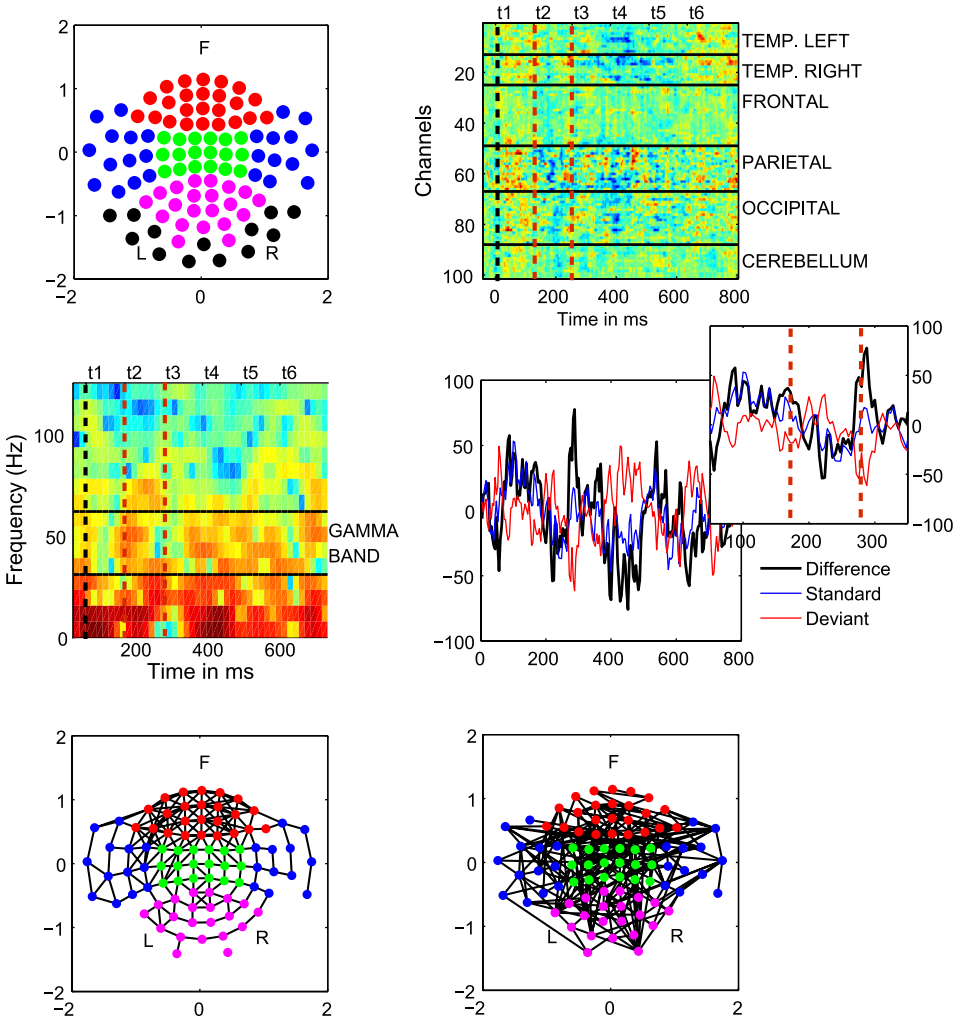

Fig. 2. Magnetoencephalography (MEG) recordings of the MMN paradigm, evoked responses, and coherency between sensors. *Top left*: the locations of the MEG sensors across the skull on an azimuthal map projection; the different colors correspond to the different lobes: temporal (blue), frontal (red), parietal (green), occipital (pink), and cerebellum (black). F, L, and R, front, left, and right orientations of the head, respectively. *Top right*: an average of the MMN response across all 14 subjects and for each 101 channels, whereas the panel below it (*middle right*) shows the average across all channels for the standard (blue), deviant (red), and difference (black) response. The *inset* details the MMN response interval by focusing in on t_2 (delimited by red dashed lines). The different time analysis intervals, t_1–t_6, are shown in all the relevant panels. *Middle left*: a spectrogram of the absolute power of the MMN signal averaged across all sensors with the gamma band (33–64 Hz) highlighted. The MMN response is evident in the time window 128–256 ms, delimited by red dotted lines, which correspond to the analysis time window t_2. *Bottom*: network for the real (*left*) and imaginary (*right*) parts of coherency, averaged for 1 subject for the standard tone and for t_1 = 1–128 ms. Note that the regular lattice of connections between neighboring sensors disclosed by analysis of the real component of coherency is attributable to volume conduction artefcats, which are mitigated substantially by analysis of the imagingary part of coherency.

MEG data acquisition. The MEG data were recorded from a 306-channel Vectorview system (Elekta Neuromag, Stockholm, Sweden), installed at the Medical Research Council Cognition and Brain Sciences Unit (Cambridge, UK), which combines two orthogonal planar gradiometers and one magnetometer at each of 102 sensor locations within a helmet-shaped array situated in a magnetically shielded room. The data were recorded at 1 kHz using a bandpass filter of 0.03–330 Hz. The position of the head, relative to the sensor array, was monitored continuously by four or five head position indicator (HPI) coils attached to the scalp.

The 204 gradiometers are made up of 102 pairs, which measure the signal in the x and y orientations, located in the plane tangent to the head. We used the root mean square value of the combined $\partial_x B_z$ and $\partial_y B_z$ signals. Assuming $B_x = B_y = 0$, this is equivalent to the electric flux in the plane of the cortex. The electric flux strength is assumed to be a measure of the mass neuronal activity in a patch of cortex immediately beneath the sensor location.

The sensors can be grouped into temporal lobe (left and right), frontal lobe, parietal lobe, occipital lobe, and cerebellar regions, based on their locations above the scalp surface (see Fig. 2). Recordings from the designated cerebellar sensors were heavily contaminated by electromyography signals attributable to neck-muscle movements, and these sensors were excluded accordingly from further analysis.

MEG data preprocessing. All raw datasets were downsampled by a factor of 4 (250 Hz) and preprocessed further to remove eye blinks, head movements, and any noise from the HPI coils [see Kitzbichler et al. (2011) for preprocessing details]. Two subjects were removed, due to presence of marked outliers in their MEG datasets, defined as one or more sensors with variance more than one order of magnitude greater than the median sensor variance, yielding an evaluable sample size of 14.

Each stimulus (standard or deviant tone) has an associated number of trials n, which can be treated as an ensemble. The signal for each trial $S_n(t)$ was defined from $t = -40$ ms to $t = 700$ ms, where $t = 1$ corresponds to the stimulus onset; epochs were corrected to the -40- to 0-ms baseline period and detrended over $t = 1$ ms to $t = 700$ ms to remove linear trends.

For both stimulus types, each trial was divided into six consecutive time epochs, t_{1-6}, each lasting ~128 ms, with the first interval time locked to the stimulus onset. This allowed us initially to examine the full-time interval between consecutive stimuli; it also allowed us to focus on the time intervals specifically corresponding to the MMN response. The epochs over all trials were then concatenated (without overlap) into a single time series, $S_m = [t_{1,m} \ldots t_{n,m}]$, where S is the concatenated signal, and m indexes the time epoch. On this basis, we can assume weak stationarity, as the window length is approximately equivalent to the MMN response time but still greater than the time scales of the involved dynamics (~5–40 ms for the gamma range).

Coherency. Coherency was used to estimate band-limited association between oscillatory activity in the signals recorded at each $\{i,j\}$ pair of sensors and is defined as

$$C_{ij} = P_{ij} / \sqrt{\left(P_{ii} P_{jj}\right)}. \tag{1}$$

$|C_{ij}|^2$ is known as the magnitude-squared coherence. P_{ij} is the cross-spectral density defined as the Fourier transform of the cross-covariance function, whereas P_{ii} and P_{jj} are the autospectral densities. P_{ij} describes how the common power content of a pair of time series, $i(t)$ and $j(t)$, varies with frequency.

$$P_{ij}(w) = \sum_{m=-\infty}^{\infty} R_{ij}(\tau) e^{-iwm} \tag{2}$$

where $R_{ij}(\tau)$ is the cross-covariance at lag τ

$$R_{ij}(\tau) = \frac{1}{L} \Sigma \left(i(t+\tau) - \langle i \rangle_t\right)\left(j(t) - \langle j \rangle_t\right) \tag{3}$$

and L is the number of points in the time series.

Coherency analysis was performed on the S_m concatenated signal using a sliding, 32-point Gaussian window with no overlap. Volume conduction effects were evident in spatially neighboring sensors, which appear strongly correlated because of their close proximity and not because of any underlying neural interaction (Fig. 2). We thus considered the imaginary part of the coherency, which contains phase information, as a measure of the biologically mediated synchronization between different processes (Nolte et al. 2004; Stam et al. 2007). In contrast to the real part of coherency, the imaginary part is not sensitive to volume conduction, as it is nonexistent for processes that have zero time-lag between them. Although the imaginary component is small, it is preferred over the phase as a synchronization measure, because noninteracting processes can produce random (not necessarily small) phase differences (Nolte et al. 2004).

MEG data analysis: network topology and connection distance. Networks were modeled as weighted or unweighted (binary) graphs constructed by a probabilistic thresholding rule (defined in more detail below, *Probabilistic thresholding and statistical analysis*) from the matrix of pairwise $Im(C_{ij})$ values for all pairs of sensors. The resulting networks were characterized in terms of the physical distance between connected sensors and standard metrics of network topology.

Physical distance was estimated by the Cartesian distance d_{ij} between sensors i and j on an azimuthal map projection of their positions on the surface of the head.

The clustering coefficient, which can be defined both locally and globally, is essentially the ratio of the geometric weight of all closed triplets (three nodes connected by three edges, denoted w_c) to the total weight of both open (three nodes only connected by two edges, denoted w_o) and closed triplets in the network (Onnela et al. 2005).

$$C = \frac{\text{total value closed triplets}}{\text{total value triplets}} = \frac{\Sigma w_c}{\Sigma w_c + \Sigma w_o} \tag{4}$$

Thus clustering can be estimated for each node (sensor) and then averaged over sensors to estimate the network mean clustering coefficient.

The efficiency (Latora and Marchiori 2001) of a network or graph G is given by

$$E(G) = \frac{1}{N(N-1)} \sum_{i \neq j} \frac{1}{l_{ij}} \tag{5}$$

where N is the number of nodes in G, and l_{ij} is the path length between nodes i and j. Nodes, which are not connected, merely contribute a zero value to $E(G)$. The global efficiency is a measure of the efficiency of the information transfer across the graph. This quantity can also be quantified locally for every node i by forming a subgraph G_i of its nearest neighbors. In this case, the average local efficiency is given by

$$E_{\text{avg}} = \frac{1}{N} \sum_i E(G_i). \tag{6}$$

Probabilistic thresholding and statistical analysis. P values were calculated for the imaginary part of coherency between each pair of sensors $Im(C_{ij})$, and the false discovery rate (FDR) was used to detect significant interactions (Benjamini and Hochberg 1995; Benjamini and Yekutieli 2001). The FDR controls for the fact that in the context of multiple comparisons, a nominally significant P value is more likely to be observed by chance than in the context of a single statistical comparison. After sorting the P values in ascending order, the maximum of the P_i, which satisfies $P_i < \alpha i / n_{\text{comp}}$, where n_{comp} is the number of comparisons, and $\alpha = 0.05$ is the probability of type I error, was found. All P values lower or equal to this maximum were regarded as significant. At this level of control, 95% of all statistically significant results are true positives.

If a pair of sensors had statistically significant $Im(C_{ij})$, an edge was drawn between the corresponding nodes in a graph representing the network interactions. The connection density of the resulting graph is

defined by the number of edges as a percentage of the maximum possible number of edges [N·(N − 1)]/2. We constructed graphs with connection density in the range 1–10%, i.e., up to the maximum connection density consistent with probabilistic thresholding of the imaginary coherency matrix at a FDR of 5%. We confirmed that the threshold value of $Im(C_{ij})$, corresponding to arbitrary connection density, was approximately equivalent for standard and deviant frequency trial data. We used identical numbers of deviant and standard trials to estimate the mean network for each trial type in each subject; the standard frequency trials chosen for analysis were those that immediately preceded the less commonly occurring deviant frequency trials.

To compare network parameters between standard and deviant frequency trial types, we controlled each individual's network to have identical connection density and number of connected nodes, we measured topological and distance metrics for each network (as described above), and we used mixed-effects ANOVA models to compare mean metrics between networks. Each ANOVA model comprised a fixed effect for trial type (standard or deviant) and a random effect for individual subjects and treated each network metric separately as a dependent variable. We defined a statistically significant difference between trial types if $P < 0.05$ for any network metric.

RESULTS

Evoked and induced responses to deviant tones. Subtraction of the response to the standard tones from the response to the deviant tones resulted in an evoked response [or event-related field (ERF)], as expected, in the form of a negative peak in the MEG signal between 100 and 250 ms after the deviant stimulus onset (Näätänen et al. 2004, 2007) (see Figs. 1 and 2). In Fig. 1, the significance of the ERF was determined by a *t*-test, corrected for multiple comparisons. Also as expected (Edwards et al. 2005; Kaiser et al. 2000; Stefanics et al. 2007), time-frequency analysis demonstrated transiently increased gamma-band power in the same time epoch (Fig. 2). We therefore focused the analysis of synchronization and functional network topology on the gamma-band frequency interval and specified time epochs for analysis that included the period 128–256 ms after stimulus presentation. Although variation-induced oscillatory power can be observed across the alpha and beta bands, the preferred time window of 128 ms, which we chose to resolve network changes, coincident with timing of the MMN response, was too short to allow dynamic network changes in these lower frequency bands to be investigated.

Global network parameters. Considering first the global network parameters estimated from the imaginary coherency between sensors in the 128- to 256-ms time epoch (Fig. 3), we found that both standard and deviant tone conditions were associated with small-world properties of gamma-band networks (high global efficiency combined with high local efficiency or clustering). This conservation of global topological parameters was observed for several different weighted variants of the clustering coefficient [binary, shortest path distance, and Cartesian distance weighting were tested, in addition to $Im(C_{ij})$]. Mean physical distance of synchronization was somewhat greater for networks recorded during deviant stimuli than during standard stimuli, but for both networks, the synchronization distance was less than in a random network. There were no statistically significant differences between stimulus types in any of these global network parameters (global clustering: $P = 0.605$; global efficiency: $P = 0.771$).

Local clustering. In Fig. 4, we show headmaps of the local clustering (local efficiency results are similar) for the standard and deviant tones, alongside a randomized signal for comparison. The temporal evolution of the network configuration averaged over subjects and epochs is shown by mapping the networks across three time epochs or intervals: $t_1 = 0$–128 ms, $t_2 = 128$–256 ms, and $t_3 = 256$–384 ms.

For clarity, the MMN-evoked response is also shown on the same timescale. The SE of the clustering coefficients was estimated as ±0.016, and statistical significance of the observed differences in clustering was assessed by ANOVA modeling. Both the deviant and standard tones were associated with localized, high clustering of connections in the brain networks compared with random networks. Significant differences between tones were most evident in the second time epoch ($t_2 = 128$–256 ms), coinciding with the MMN-evoked response. In this epoch, there was significantly increased clustering in the temporal lobe, more specifically, in the left

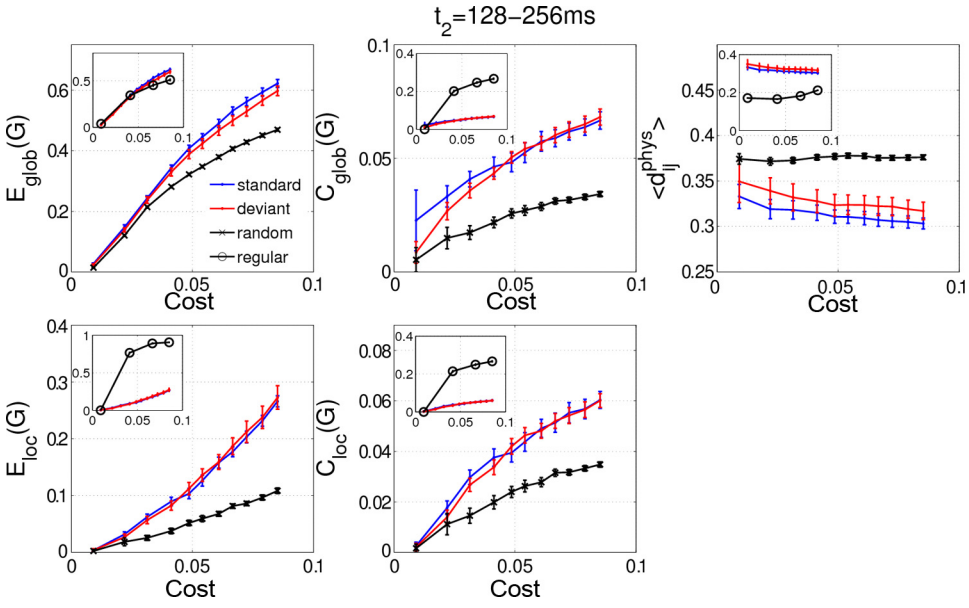

Fig. 3. Topological properties of gamma-band functional networks derived from MEG recordings during the MMN paradigm. Global efficiency [$E_{glob}(G)$; *top left*], global clustering [$C_{glob}(G)$; *top middle*], local efficiency [$E_{loc}(G)$; *bottom left*], local clustering [$C_{loc}(G)$; *bottom right*], and total physical network distance [$<d_{ij}^{phys}>$; *top right*], averaged across all subjects for standard (blue) and deviant tones (red), as well as regular (black "○"; shown in figure insets) and randomized datasets (black "×"). (G) refers to the graph or network. The error bars correspond to the SE across subjects. The time interval considered is $t_2 = 128$–256 ms.

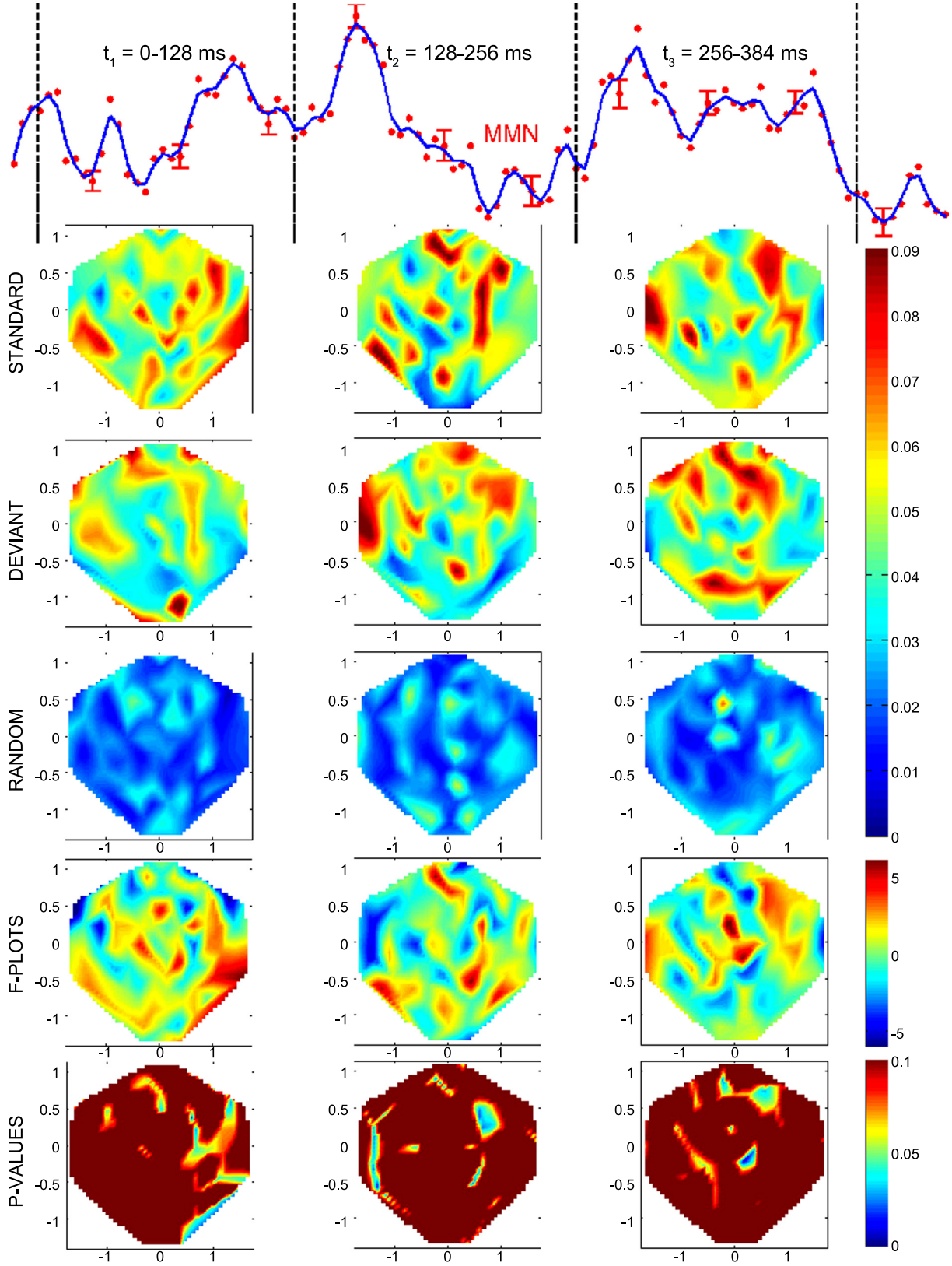

Fig. 4. Time-resolved, stimulus-related differences in functional network topology. The local clustering coefficient for t_1–t_3 for the standard, deviant, and random tones is represented for networks with connection density = 6%. The average MMN response over all channels and subjects for the same time intervals is shown along the top panel of the figure. A random-effects ANOVA model is used to determine significantly different means ($P < 0.05$) of the clustering coefficient between networks recorded, following presentation of standard tones (2nd row) and deviant tones (3rd row) and the randomized dataset (4th row). The F values are positive when $C_{loc,standard}(G) > C_{loc,deviant}(G)$ and negative when $C_{loc,standard}(G) < C_{loc,deviant}(G)$. These maps highlight greater local clustering in both brain networks compared with random networks and the emergence of significant local clustering in the left temporal region during the 128- to 256-ms epoch following presentation of deviant tones.

temporal lobe (midtemporal channel: F = 5.67, P = 0.009, df = 1, 13), for the deviant tone network, whereas there was significantly increased clustering in frontal regions for the standard tone network (midfrontal channel: F = 4.45, P = 0.022, df = 1, 13).

Interlobar synchronization. In networks derived from both deviant and standard frequency trials, we found that interlobar, relatively long-distance connections were frequent between sensors located over different lobes of the brain. However, in deviant tone-related networks, there was a significant increase in the proportion of long-distance, interlobar connections, specifically during the 128- to 256-ms epoch, as can be seen in Fig. 5. If we define r as the ratio of inter- to intralobar edges, we find that over this epoch, r_{dev} = 2.55 ± 0.20, and r_{stand} = 2.03 ± 0.11 (P = 0.036). In particular, there was a high proportion of connections between right and left temporal lobes (Fig. 5) in the deviant tone-related network in the time epoch coinciding with the MMN response. In contrast, the standard tone-related network showed a high density of short-range, intralobar connections in the frontal lobe, consistent with the high clustering also observed in that area.

DISCUSSION

We have used topological and physical network parameters to map human brain functional network reconfiguration dynamically over the course of ~1 s, following acoustic presentation of standard or deviant frequency tones. This experimental paradigm has been used to evoke a negative deflection in the average MEG (or EEG) signal amplitude, the so-called MMN,

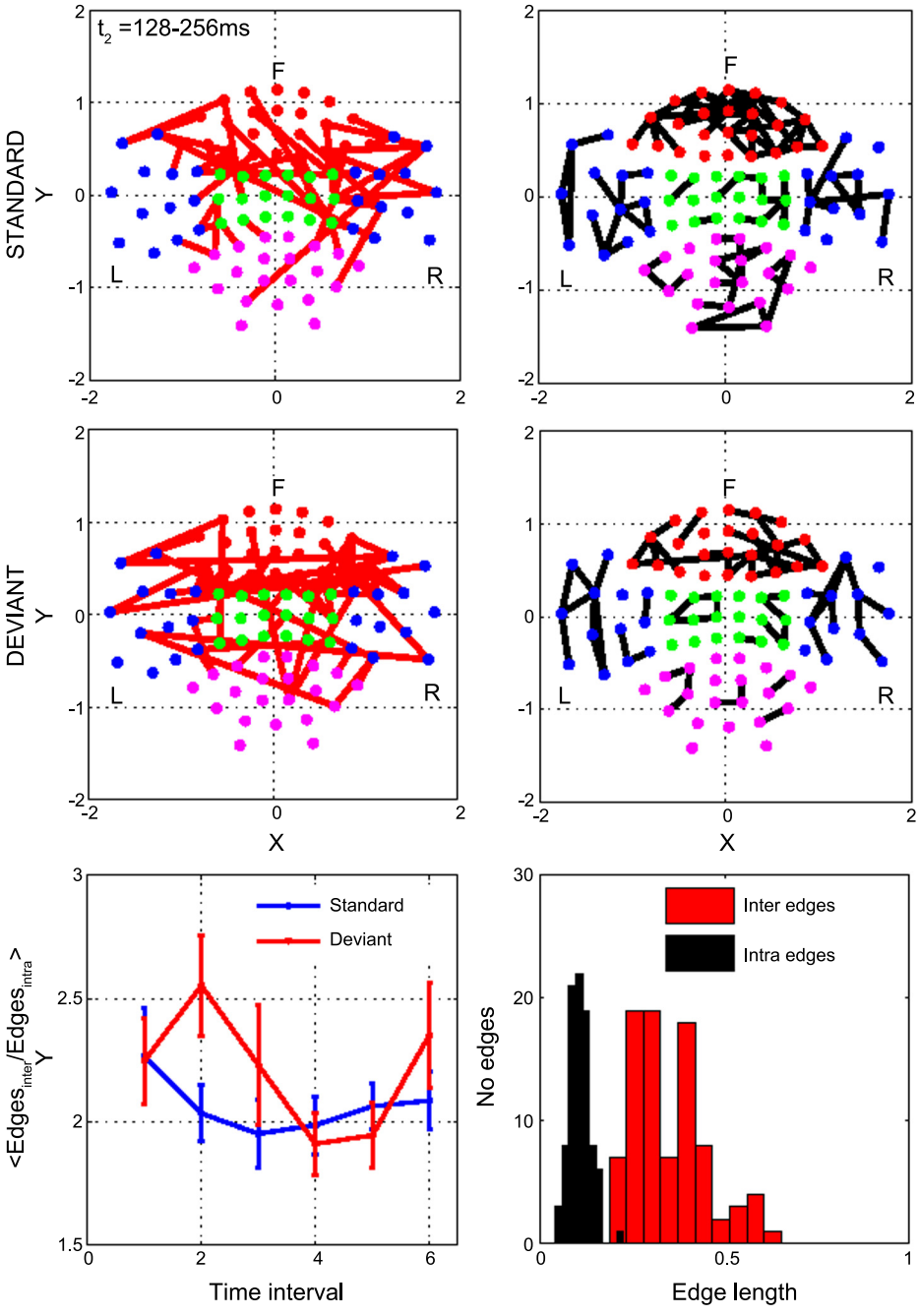

Fig. 5. Task-related changes in long-distance, interlobar synchronization. Interlobar (red) and intralobar (black) connections for the standard (*top panels*) and deviant (*middle panels*) tones for t_2 = 128–256 ms and connection density = 6%. The interlobar connections correspond to connections among lobes: temporal (blue), frontal (red), parietal (green), and occipital (pink), whereas the intralobar connections are contained within a single lobe. *Bottom left*: ratio of inter- to intralobe edges averaged across all subjects. *Bottom right*: histogram of the physical length of the edges (normalized to the maximum node separation) for the deviant tone during t_2. The histogram shows that the interlobar edges correspond to longer-range connections ($<d_{ij,inter}>$ ~0.4) than the intralobar edges ($<d_{ij,intra}>$ ~0.1) and that there is a greater number of these long-range connections following presentation of deviant tones.

which occurs ~125–250 ms after presentation of the deviant stimulus (Näätänen et al. 2004). Functional connectivity determined by the statistical interdependence of both local and remote cortical activity (Varela et al. 2001) is highly complementary to localizationist analysis of neurophysiological data and gives valuable insight into human brain functioning (Aertsen et al. 1989; Bressler 2002; Reijneveld et al. 2007; Singer 1999; Tononi and Edelman 1998; Varela et al. 2001). However, to the best of our knowledge, this is the first study of the MMN paradigm to have investigated the brain's response to deviant stimuli in terms of topological parameters estimated by graph theoretical modeling of brain functional networks.

We used the imaginary part of coherency between sensors as the basis for building functional networks, because it has been shown (Nolte et al. 2004; Stam et al. 2007) (and we confirmed; Fig. 2) that the real part and the magnitude-squared coherency are heavily dominated by volume-conduction effects, represented topologically by a lattice of connections with zero time-lag. By considering exclusively the imaginary part, we expect to see phase-shifted associations between sensors that are more likely to represent biologically interesting interactions between underlying neuronal populations. This technique, therefore, allowed us to mitigate the impact of volume conduction artefacts on functional networks constructed from scalp sensor recordings.

We found that global network parameters, such as clustering and efficiency, were indistinguishable within errors for the standard and deviant tone-related networks. In other words, the global network topology had a roughly constant level of complexity, independent of task conditions. The observed network nevertheless displayed properties distinct from equivalent random and regular network models, such as a clustering coefficient higher than the random model, yet lower than for a comparable regular network. This is consistent with previous work, suggesting that nonrandom or small-world properties are highly conserved global properties of brain networks (Bullmore and Bassett 2011; Bullmore and Sporns 2009).

On the other hand, there were consistent differences between the standard and deviant tone-related networks in terms of more topologically or spatially local parameters. In the time interval where the MMN-evoked response was observed, there was significantly increased efficiency of left temporal sensors, and there was a significant global increase in the proportion of long-distance interlobar edges in the deviant tone-related network compared with the standard tone-related network. Efficiency of information transfer between left temporal regions and the rest of the network was increased, due to greater local clustering of connections in the temporal cortex and the emergence of long-range connections between left temporal cortex and other cortical areas, including interhemispheric connections to the right temporal lobe.

These novel observations are compatible with prior theoretical predictions. For example, neuronal workspace theory predicts that more salient sensory stimuli, with greater access to conscious representation, should be associated with the formation of dynamically coherent, integrated ensembles or workspaces of neurons, which may be located in distantly separated anatomical regions (Baars 1988; Dehaene 2001). High efficiency of information transfer between a distributed set of cortical regions is predicted by workspace theory to provide a physiological substrate for integrative processing of salient stimuli or effortful cognitive processes (Shanahan 2010). Our findings of increased network efficiency and greater (long-distance) interlobar synchronization in response to more salient acoustic stimuli are consistent with this theoretical position. Moreover, these data corroborate and extend previous graph theoretical studies, demonstrating that workspace reconfiguration of MEG networks can be demonstrated in response to variable degrees of conscious, cognitive effort over relatively long (~2 s) experimental trials (Kitzbichler et al. 2011).

In the future, it will be interesting to further explore how the network changes related to deviant stimulation might also be quantified by changes in the community structure or modularity of the network (Meunier et al. 2010). Workspace theory would predict that the long-distance connections between anatomically distinct lobes, which we have reported in response to deviant stimuli, have the topological effect of "breaking modularity" (Dehaene 2001). In other words, anatomically interlobar connections are often also expected to be topologically intermodular connections. However, this prediction has not been tested formally by a topological analysis of network modularity in these data.

This pattern of graph theoretical results, comprising both local changes in clustered connectivity between a clique of topologically and spatially neighboring nodes in the left temporal cortex, as well as more distributed changes in the strength of long-distance synchronization between frontal and temporal areas, is arguably also compatible with recent experimental and modeling studies of the MMN response (Garrido et al. 2009b; Näätänen et al. 2007). Several prior studies using dipole modeling have implicated frontal and temporal cortical generators of the MMN-evoked response (Näätänen et al. 2007). The anatomical distribution of topological changes in our data is compatible with these dipole analyses, as well as with other modeling approaches to the MMN, which have considered its generation in the theoretical context of network interactions rather than local generators.

For example, studies using DCM have provided evidence that the brain system's phenotype of unexpected auditory stimulation includes both interareal plasticity, as predicted by the model adjustment theory, and intra-areal changes in temporal cortex, as predicted by the adaptation theory (Garrido et al. 2008). The topological and spatial changes in network configuration, which we have described as part of the MMN response, are conceptually convergent, with the more general theory that prediction errors generated by surprising stimuli may drive both local and interareal changes in synaptic connectivity (Garrido et al. 2009a). It could be useful in the future to combine graph theoretical and DCM approaches to analysis of brain system changes to disruptive or unpredicted sensory stimuli. It is expected that the network changes, which we have demonstrated in response to deviant auditory stimuli, will prove to be compatible with prior models of the MMN-evoked response as a marker of prediction error (Baldeweg 2006, 2007).

Graph theoretical analysis of MEG networks in general will also likely be advanced further by developments in anatomical localization of network nodes to allow more direct integration of topological properties with dipole modeling results. However, it is also important to acknowledge that the "classical" analysis of the MMN-evoked response has focused on a lower frequency interval (~3–30 Hz) than the gamma frequency

interval considered here; so, there are methodological differences in frequency interval as well as spatial localization to consider in assessing these results in relation to the prior literature about the MMN-evoked response. We note that gamma-band oscillations have been implicated repeatedly in a wide variety of cognitive and sensory processes (Fell et al. 2001; Kaiser and Lutzenberger 2003; Micheloyannis et al. 2003; Sarnthein et al. 1998), including feature binding or stimulus identification processes (Rodriguez et al. 1999). Such a process of feature extraction, identification, and binding is certainly necessary to identify deviance in the incoming auditory stimulation. So, it is novel but not theoretically unexpected that deviant auditory stimulus presentation should be associated with changes in coherent oscillatory activity in the gamma-band frequency interval. Importantly, previous studies pointed toward an interplay between gamma- and beta-band oscillations in the detection of deviant auditory stimuli and possibly also in the generation of the MMN-evoked response (Haenschel et al. 2000).

Conclusion. We have examined changes in brain functional network properties elicited by deviant frequency tones acoustically presented in the MMN paradigm, using MEG to resolve dynamic changes in synchronization of high-frequency (gamma band; 33–64 Hz) oscillations. Global topological parameters were conserved between the networks corresponding to standard and deviant frequency stimuli. However, there were changes in local efficiency or clustering of left temporal cortex and in strength of long-distance or interlobar connections between temporal and frontal cortex. These results are compatible with prior theories of brain-network reconfiguration in response to surprising or salient stimuli and show that rapid changes in network organization can be resolved by graph theoretical analysis of MEG data.

GRANTS

R. M. Nicol acknowledges the financial support of the Engineering and Physical Sciences Research Council. The experimental study was sponsored by GlaxoSmithKline and conducted at the Medical Research Council Cognition and Brain Sciences Unit (Cambridge, UK).

DISCLOSURES

The authors declare that they have no competing financial interests. E. T. Bullmore is employed half-time by GlaxoSmithKline and half-time by the University of Cambridge.

AUTHOR CONTRIBUTIONS

Author contributions: S.C.C., P.J.N., Y.S., and E.T.B. conception and design of research; M.L.S. performed experiments; R.M.N., S.C.C., and P.E.V. analyzed data; R.M.N., S.C.C., P.E.V., and E.T.B. interpreted results of experiments; R.M.N. prepared figures; R.M.N. drafted manuscript; R.M.N., S.C.C., P.E.V., P.J.N., M.L.S., Y.S., and E.T.B. edited and revised manuscript; R.M.N., S.C.C., P.E.V., P.J.N., M.L.S., Y.S., and E.T.B. approved final version of manuscript.

REFERENCES

Achard S, Salvador R, Whitcher B, Suckling J, Bullmore ET. A resilient, low-frequency, small-world human brain functional network with highly connected association cortical hubs. *J Neurosci* 3: e17, 2006.

Aertsen AM, Gerstein GL, Habib MK, Palm G. Dynamics of neuronal firing correlation: modulation of "effective connectivity". *J Neurosci* 61: 900–917, 1989.

Alho K. Cerebral generators of mismatch negativity (MMN) and its magnetic counterpart (MMNm) elicited by sound changes. *Ear Hear* 16: 38–51, 1995.

Baars BJ. *A Cognitive Theory of Consciousness*. Cambridge University Press, UK, 1988.

Baldeweg T. ERP repetition effects and mismatch negativity generation: a predictive coding perspective. *J Psychophysiol* 21: 204–213, 2007.

Baldeweg T. Repetition effects to sounds: evidence for predictive coding in the auditory system. *Trends Cogn Sci* 10: 93–94, 2006.

Barabási AL, Albert R. Emergence of scaling in random networks. *Science* 286: 509–512, 1999.

Barabási AL, Albert R, Jeong H. Scale-free characteristics of random networks: the topology of the world wide-web. *Physica A* 281: 69–77, 2000.

Bassett DS, Bullmore ET. Small-world brain networks. *Neuroscientist* 12: 512–523, 2006.

Bassett DS, Greenfield DL, Meyer-Lindenberg A, Weinberger DR, Moore SW, Bullmore, ET. Efficient physical embedding of topologically complex information processing networks in brains and computer circuits. *PLoS Comput Biol* 6: e1000748, 2010.

Bassett DS, Meyer-Lindenberg A, Achard S, Duke T, Bullmore ET. Adaptive reconfiguration of fractal small-world human brain functional networks. *Proc Natl Acad Sci USA* 3: 19518–19523, 2006.

Benjamini Y, Hochberg Y. Controlling the false discovery rate: a practical and powerful approach to multiple testing. *J Roy Stat Soc B,* 57: 289–300, 1995.

Benjamini Y, Yekutieli D. The control of the false discovery rate in multiple testing under dependency. *Ann Stat* 29: 1165–1188, 2001.

Bressler S. Understanding cognition through large-scale cortical networks. *Curr Dir Psychol Sci* 11: 58–61, 2002.

Bullmore ET, Bassett DS. Brain graphs: graphical models of the human brain connectome. *Annu Rev Clin Psychol* 7: 113–140, 2011.

Bullmore ET, Sporns O. Complex brain networks: graph theoretical analysis of structural and functional systems. *Nat Rev Neurosci* 10: 186–198, 2009.

Chialvo DR. Emergent complex neural dynamics. *Nat Phys* 6: 744–750, 2010.

Dehaene S. *The Cognitive Neuroscience of Consciousness*, The MIT Press, Londres, Angleterre, 2001.

Edwards E, Soltani M, Deouell LY, Berger MS, Knight RT. High gamma activity in response to deviant auditory stimuli recorded directly from human cortex. *J Neurophysiol* 94: 269–280, 2005.

Eguíluz V, Chialvo D, Cecchi G, Apkarian A. Scale-free brain functional networks. *Phys Rev Lett* 94: 018102, 2005.

Erdös P, Rényi AR. On random graphs. *Publ Math Debrecen* 6: 290–291, 1959.

Fell J, Klaver P, Lehnertz K, Grunwald T, Schaller C, Elger CE, Fernández G. Human memory formation is accompanied by rhinal-hippocampal coupling and decoupling. *Nat Neurosci* 4: 1259–1264, 2001.

Garagnani M, Shtyrov Y, Pulvermuller F. Effects of attention on what is known and what is not: MEG evidence for functionally discrete memory circuits. *Front Hum Neurosci* 3: 10, 2009.

Garrido MI, Friston KJ, Kiebel SJ, Stephan KE, Baldeweg T, Kilner JM. The functional anatomy of the MMN: a DCM study of the roving paradigm. *Neuroimage* 42: 936–944, 2008.

Garrido MI, Kilner JM, Kiebel SJ, Friston KJ. Dynamic causal modeling of the response to frequency deviants. *J Neurophysiol* 101: 2620–2631, 2009a.

Garrido MI, Kilner JM, Stephan KE, Friston KJ. The mismatch negativity: a review of underlying mechanisms. *Clin Neurophysiol* 120: 453–463, 2009b.

Haenschel C, Baldeweg T, Croft RJ, Whittington M, Gruzelier J. Gamma and beta frequency oscillations in response to novel auditory stimuli: a comparison of human electroencephalogram (EEG) data with in vitro models. *Proc Natl Acad Sci USA* 97: 7645–7650, 2000.

Hagmann P, Cammoun L, Gigandet X, Meuli R, Honey CJ, Wedeen VJ, Sporns O. Mapping the structural core of human cerebral cortex. *PLoS Biol* 6: e159, 2008.

Hämäläinen M, Hari R, Ilmoniemi RJ, Knuutila J, Lounasmaa OV. Magnetoencephalography—theory, instrumentation, and applications to noninvasive studies of the working human brain. *Rev Mod Phys* 65: 413–497, 1993.

Kaiser J, Lutzenberger W. Induced gamma-band activity and human brain function. *Neuroscientist* 9: 475–484, 2003.

Kaiser J, Lutzenberger W, Preissl H, Ackermann H, Birbaumer N. Right-hemisphere dominance for the processing of sound-source lateralization. *J Neurosci* 20: 6631–6639, 2000.

Kitzbichler MG, Henson RNA, Smith ML, Nathan PJ, Bullmore ET. Cognitive effort drives workspace configuration of human brain functional networks. *J Neurosci* 31: 8259–8270, 2011.

Kujala T. The role of early auditory discrimination deficits in language disorders. *J Psychophysiol* 21: 239–250, 2007.

Kujala T, Näätänen R. The adaptive brain: a neurophysiological perspective. *Prog Neurobiol* 91: 55–67, 2010.

Latora V, Marchiori M. Efficient behavior of small-world networks. *Phys Rev Lett* 87: 198701, 2001.

Meunier D, Lambiotte R, Fornito A, Ersche KD, Bullmore ET. Hierarchical modularity in human brain functional networks. *Front Neuroinform* 3: 37, 2010.

Micheloyannis S, Vourkas M, Bizas M, Simos P, Stam CJ. Changes in linear and nonlinear EEG measures as a function of task complexity: evidence for local and distant signal synchronization. *Brain Topogr* 14: 239–247, 2003.

Näätänen R, Gaillard AWK, Mäntysalo S. Early selective-attention effect on evoked potential reinterpreted. *Acta Psychol (Amst)* 42: 313–329, 1978.

Näätänen R, Paavilainen P, Rinne T, Alho K. The mismatch negativity (MMN) in basic research of central auditory processing: a review. *Clin Neurophysiol* 118: 2544–2590, 2007.

Näätänen R, Pakarinen S, Rinne T, Takegata R. The mismatch negativity (MMN): towards the optimal paradigm. *Clin Neurophysiol* 115: 140–144, 2004.

Newman MEJ. The structure and function of complex networks. *SIAM Review* 45: 167–256, 2003.

Nolte G, Bai O, Wheaton L, Mari Z, Vorbach S, Hallett M. Identifying true brain interaction from EEG data using the imaginary part of coherency. *Clin Neurophysiol* 115: 2292–2307, 2004.

Onnela JP, Saramäki J, Kertész J, Kaski K. Intensity and coherence of motifs in weighted complex networks. *Phys Rev E Nonlin Soft Matter Phys* 71: 065103, 2005.

Palva JM, Monto S, Kulashekhar S, Palva S. Neuronal synchrony reveals working memory networks and predicts individual memory capacity. *Proc Natl Acad Sci USA* 107: 7580–7585, 2010a.

Palva S, Monto S, Palva JM. Graph properties of synchronized cortical networks during visual working memory maintenance. *Neuroimage* 49: 3257–3268, 2010b.

Pekkonen E, Jousmäki V, Könönen M, Reinikainen K, Partanen J. Auditory sensory memory impairment in Alzheimer's disease: an event-related potential study. *Neuroreport* 5: 2537–2540, 1994.

Reijneveld JC, Ponten SC, Berendse HW, Stam CJ. The application of graph theoretical analysis to complex networks in the brain. *Clin Neurophysiol* 118: 2317–2331, 2007.

Rodriguez E, George N, Lachaux JP, Martinerie J, Renault B, Varela FJ. Perception's shadow: long-distance synchronization of human brain activity. *Nature* 397: 430–433, 1999.

Salvador R, Suckling J, Coleman MR, Pickard JD, Menon D, Bullmore ET. Neurophysiological architecture of functional magnetic resonance images of human brain. *Cereb Cortex* 15: 1332–1342, 2005.

Sarnthein J, Petsche H, Rappelsberger P, Shaw GL, von Stein A. Synchronization between prefrontal and posterior association cortex during human working memory. *Proc Natl Acad Sci USA* 95: 7092–7096, 1998.

Shanahan M. *Embodiment and the Inner Life: Cognition and Consciousness in the Space of Possible Minds.* Oxford University Press, UK, 2010.

Shelley AM, Silipo G, Javitt DC. Diminished responsiveness of ERPs in schizophrenic subjects to changes in auditory stimulation parameters: implications for theories of cortical dysfunction. *Schizophr Res* 37: 65–79, 1999.

Shelley AM, Ward PB, Catts SV, Michie PT, Andrews S, McConaghy N. Mismatch negativity: an index of a preattentive processing deficit in schizophrenia. *Biol Psychiat* 30: 1059–1062, 1991.

Singer W. Neuronal synchrony: a versatile code for the definition of relations?. *Neuron* 24: 49–65, 1999.

Stam CJ, Nolte G, Daffertshofer A. Phase lag index: assessment of functional connectivity from multi channel EEG and MEG with diminished bias from common sources. *Hum Brain Mapp* 28: 1178–1193, 2007.

Stefanics G, Háden G, Huotilainen M, Balázs L, Sziller I, Beke A, Fellman V, Winkler I. Auditory temporal grouping in newborn infants. *Psychophysiology* 44: 697–702, 2007.

Tononi G, Edelman GM. Consciousness and the integration of information in the brain. *Adv Neurol* 77: 245–279, 1998.

Varela F, Lachaux JP, Rodriguez E, Martinerie J. The brainweb: phase synchronization and large-scale integration. *Nat Rev Neurosci* 2: 229–239, 2001.

Watts DJ, Strogatz SH. Collective dynamics of "small-world" networks. *Nature* 393: 440–442, 1998.